
Article:
LAIRD, ALISON MONICA orcid.org/0000-0003-0423-363X, ANGUS, CAMERON, Kay, B et al. (3 more authors) (2025) Inverse kinematics study of the energy levels of Ne21 populated with the Ne20+d reaction. Physical Review C - Nuclear Physics. 025803. ISSN: 2469-9993

https://doi.org/10.1103/byw8-bvrn

Inverse kinematics study of the energy levels of ^{21}Ne populated with the ^{20}Ne $+d$ reaction

C. Angus,[1,2] A. M. Laird,[1] T. L. Tang,[3,4] P. Adsley,[5,6] M. L. Avila,[3] S. Chakraborty,[1,*] J. Frost-Schenk,[1,†] C. R. Hoffman,[3] H. Jayatissa,[3,‡] B. P. Kay,[3] R. Longland,[7,8] C. Müller-Gatermann,[3] J. S. Rojo,[1,*] I. A. Tolstukhin,[3] and G. L. Wilson[9,3,§]

[1]*School of Physics, Engineering and Technology, University of York, York YO10 5DD, England, United Kingdom*
[2]*TRIUMF, 4004 Wesbrook Mall, Vancouver, British Columbia V6T 2A3, Canada*
[3]*Physics Division, Argonne National Laboratory, 9700 South Cass Avenue, Lemont, Illinois 60439, USA*
[4]*Department of Physics, Florida State University, Tallahassee, Florida 32306, USA*
[5]*Cyclotron Institute, Texas A&M University, College Station, Texas 77843, USA*
[6]*Department of Physics and Astronomy, Texas A&M University, College Station, Texas 77843, USA*
[7]*Department of Physics, North Carolina State University, Raleigh, North Carolina 27695, USA*
[8]*Triangle Universities Nuclear Laboratory, Durham, North Carolina 27708, USA*
[9]*Department of Physics and Astronomy, Louisiana State University, Baton Rouge, Louisiana 70803, USA*

(Received 11 April 2025; accepted 7 July 2025; published 8 August 2025)

Background: In recent years there has been significant experimental effort aimed at studying the impact of ^{16}O neutron poisoning on the weak *s* process in rotating massive stars. Improving the understanding of energy levels in ^{21}Ne is crucial to reducing uncertainties in the rates of the α-induced reactions on ^{17}O that determine the overall efficiency of the weak *s* process.
Purpose: This paper reports on one such experiment: a study of the ^{20}Ne$(d, p)^{21}$Ne reaction in inverse kinematics.
Methods: Deduced spin-parity assignments were made based on adiabatic distorted-wave approximation analysis and neutron partial widths were estimated by comparison with a previous experiment.
Results: Of particular significance for nuclear astrophysics is the resulting neutron partial width for the 7820-keV energy level, estimated to be 12 200(2900) eV, and an upper limit of $\leqslant$9300 eV for that of the 7749-keV energy level.
Conclusions: These results are in tension with previous studies and therefore this paper also discusses the current state of the research into the astrophysically relevant energy levels and highlights both areas of agreement and areas of disagreement between this and various other studies that have investigated this nucleus.

DOI: 10.1103/byw8-bvrn

I. INTRODUCTION

Approximately half of elements heavier than iron are thought to be made in the slow (*s*-)neutron capture process [1]. The astrophysical sites for the *s* process are postulated to be both massive stars ($>8M_\odot$) and asymptotic giant branch stars, where the conditions mean that the neutron-capture rate for seed nuclei is generally slower than the rate of β decay. Under these conditions, pathways of nucleosynthesis lie close to the valley of stability. In massive stars the ^{22}Ne$(\alpha, n)^{25}$Mg reaction is the main source of neutrons for the *s* process and is activated at the end of He-core burning [2]. The *s* process requires seed nuclei to capture these emitted neutrons. Such seeds must be produced in other astrophysical sites, hence the *s* process is considered a secondary process. Under ordinary conditions the *s* process is not expected to have contributed significantly to the chemical makeup of the very old ultrametal poor (UMP) stars, the composition of which should be dominated by elements made in the rapid (*r*-)neutron capture process. However, where the *s* process occurs in rapidly rotating metal-poor massive stars, it is possible that a weak *s* process is efficient enough at early times to significantly contribute to nucleosynthesis and enrich the composition of UMP stars [3].

Rotation in massive stars boosts ^{14}N production by mixing ^{12}C, produced in the He-burning core, into the star's H-burning shell. The ^{14}N in turn, through a series of

*Present Address: TRIUMF, 4004 Wesbrook Mall, Vancouver, British Columbia V6T 2A3, Canada.
†Present Address: Department of Physics and Astronomy, University College London, London WC1E 6BT, England, United Kingdom.
‡Present Address: Los Alamos National Laboratory, Los Alamos, New Mexico 87545, USA.
§Present Address: United Kingdom Atomic Energy Authority, Culham Campus, Abingdon OX14 3DB, England, United Kingdom.

α-induced reactions, boosts the ^{22}Ne$(\alpha, n)^{25}$Mg reaction rate [2]. Such a process could explain the abundances of intermediate-mass elements found in UMP stars, abundances which are increased relative to *r*-process predictions [4].

The weak *s*-process in massive stars is in competition for neutrons with ^{16}O, a neutron poison [5]. ^{16}O captures neutrons in the ^{16}O$(n, \gamma)^{17}$O reaction, thus denying them to the *s*-process. The reaction ^{17}O$(\alpha, n)^{20}$Ne recycles those neutrons lost to ^{16}O [2]. However, it too is in competition with another reaction: ^{17}O$(\alpha,\gamma)^{21}$Ne. Recent studies have shown that a sufficient number of neutrons are recycled by ^{17}O$(\alpha, n)^{20}$Ne to feed the *s*-process in the convective He-burning core of rotating metal-poor stars and therefore produce a significant quantity of intermediate mass elements at early times in the universe [6]. These results partially explain the overabundance of elements $26 < Z < 47$ relative to *r*-process predictions that have been observed in UMP stars [7]. Nevertheless, there remains a significant uncertainty on the ratio of the reaction rates of ^{17}O$(\alpha, n)^{20}$Ne to ^{17}O$(\alpha,\gamma)^{21}$Ne in the energy range for He-core burning [8], which falls between 0.2 and 0.3 GK. Since in this astrophysical site both reactions proceed through narrow resonances, information on the parameters of the energy levels of the compound ^{21}Ne nucleus is needed to accurately calculate reaction rates. Therefore, energy levels with unknown or uncertain spin parities and/or partial widths can have a significant impact on the final predictions of the nucleosynthesis. In particular, the 7749- and 7820-keV energy levels of ^{21}Ne sit above both the neutron threshold at 6761.16(4) keV and the α threshold at 7347.93(4) keV and are within the Gamow window (7.652–7.985 MeV) for this site and, through their respective resonances, may play a significant role in determining the rate of the ^{17}O$(\alpha, n)^{20}$Ne reaction [6]. The current literature disagrees on the spin-parity (J^π) assignment for the 7820-keV state, with some studies reporting $2J^\pi = (3, 5)^+$ [6] and others reporting $2J^\pi = 7^-$ [8]. The spin of the 7749-keV state remains unknown.

A previous experiment, conducted in forward kinematics at TUNL using the Enge split-pole spectrometer [9], studied the ^{20}Ne$(d, p)^{21}$Ne reaction in order to determine the spin, parities, and neutron widths of ^{21}Ne energy levels at and around the astrophysically relevant energies [6]. That study, albeit having excellent *Q*-value resolution, suffered from target contamination, particularly from ^{16}O which resulted in the population of states in ^{17}O that obscured parts of the ^{21}Ne proton energy spectrum.

To resolve the issue of target contamination, an experiment measuring the ^{20}Ne$(d, p)^{21}$Ne reaction has been conducted at Argonne National Laboratory (ANL) using the HELIOS spectrometer [10]. This experiment was conducted in inverse kinematics, which resolves the issues arising from target contamination. This study also provides an interesting comparison of two experimental techniques (forward kinematics vs inverse kinematics) and shows the advantages of combining both techniques to study the same nucleus. Results from the HELIOS study are reported herein and a more general overview of the current state of research into the energy levels of the ^{21}Ne nucleus that are relevant for the weak *s* process is given. Agreements between the various studies are noted and any disagreements between studies are highlighted along with any energy levels that still have unknown spectroscopic parameters.

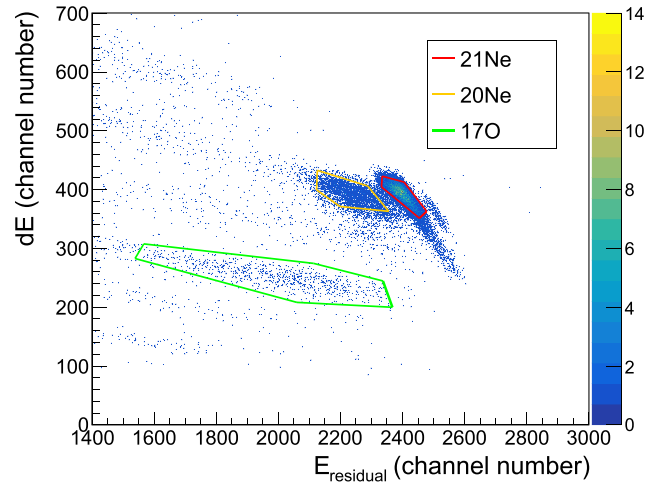

FIG. 1. Recoil gates for each nucleus studied. These data represent one of the four recoil $\Delta E/E_{\text{residual}}$ detector segments. The additional locus on the shoulder of ^{21}Ne is the scattered beam. The remaining, sparsely populated loci are ions with different *Z* numbers, *Z* increasing with ΔE.

II. EXPERIMENTAL METHOD

A beam of ^{20}Ne ions was accelerated by the Argonne Tandem-Linac Accelerator System (ATLAS) to 11 MeV/u and impinged upon a deuterated polyethylene target with an areal density of 54(1) μg/cm^2.

HELIOS is a solenoidal spectrometer of the type described in Ref. [11]. In this experiment the magnetic field was set to 2 T. Outgoing protons from the reaction were detected with an on-axis position-sensitive silicon detector array, which in this reaction subtended center-of-mass angles approximately 15° to 40° (89° to 135° in the laboratory frame). This array provided both *z*-position and energy information for each measured proton, and from these the angle of emission and excitation energy of the populated levels were calculated [10]. The experiment also utilized an additional silicon telescope downstream of the array to detect recoils in coincidence with the ejected protons. This recoil detector provided $\Delta E/E$ measurements, which could be used to identify specific recoiling nuclei and allowed a gate to be placed on the recoil used for coincidence measurements, in this case ^{21}Ne and ^{20}Ne. The recoil detector is divided into four sectors, each providing $\Delta E/E$ measurements. An example of the recoil gates for one of the detector sectors is shown in Fig. 1.

By probing the ^{21}Ne energy levels with the (d, p) reaction, high-spin (large ℓ-transfer) levels were not populated with any significant yield, since the angular momentum transfer in (d, p) reactions is low compared to other types of transfer reaction. The low probability for the population of high spin-parity states allowed those of interest, such as 7820 keV, to be treated as almost isolated. Isolating states of interest was necessary, given the low resolution that an inverse kinematics

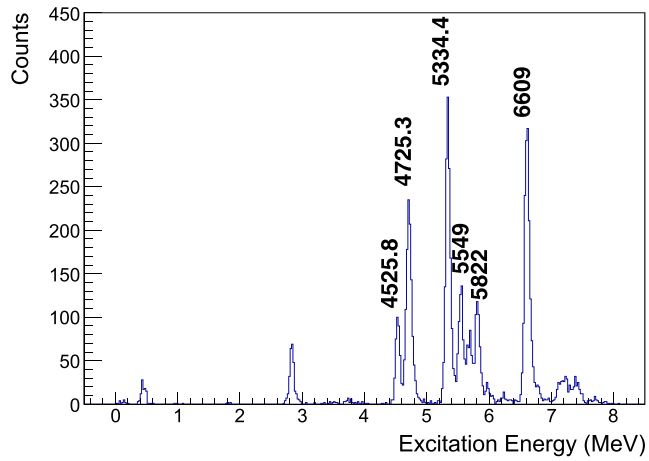

FIG. 2. The proton energy spectrum of detector 6 from the Si array with those states used for energy calibration labeled, gated on ^{21}Ne, ^{20}Ne, and ^{17}O recoils.

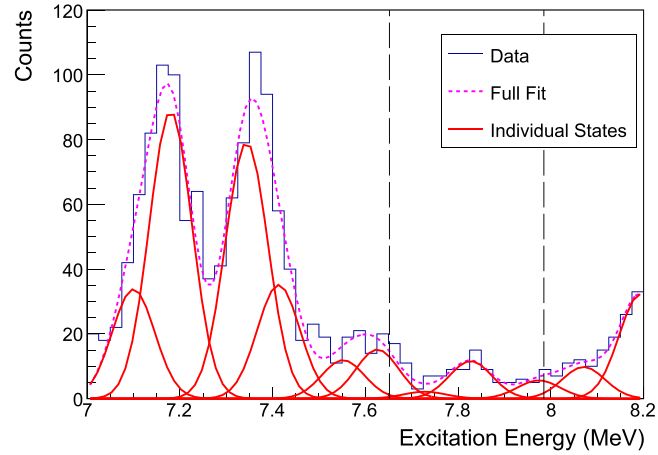

FIG. 3. The proton energy spectrum from detector 13 from the Si array, gated on ^{21}Ne, ^{20}Ne, and ^{17}O recoils and fitted above the neutron threshold. The magenta line indicates the overall fit, and the red peaks represent the fits for individual energy levels. The dashed black lines bracket the region of astrophysical interest, some of which were obscured by contaminants in previous measurements.

experimental setup offers (with respect to forward kinematics), and allowed the results to be compared with the analysis from other experiments [6,12].

III. DATA ANALYSIS

The proton-sensitive silicon detectors of the on-axis array were gain matched and calibrated using an internal calibration based on previous (d, p) studies [6,12]. The prominent states below the neutron threshold were selected for the internal calibration. Those used were 6609.0(10), 5822(2), 5549(2), 5334.4(10), 4725.35(3), and 4525.84(24) keV and are shown labeled on Fig. 2. These states were chosen since they were strongly populated, are well known, and covered a large range of energies. Once calibrated, the proton energy spectra could be used to extract observed yields for each state by fitting the spectral peaks with Gaussian functions. Fits for these strongly populated states, which are known to be narrow [13], were used to determine the resolution of protons in each detector, which varied for the 24 Si detectors in the array. Some detectors had good resolution, as low as 37 keV at full width at half maximum (FWHM). Other detectors had a much poorer resolution, up to 88 keV. Figure 2 shows an example proton spectrum from one of the detectors on the array.

The detector resolution placed constraints on the width of the peaks fitted at the Gamow window, which had much lower statistics than other regions of the spectrum and had a higher energy level density. By combining the measured detector resolution and the precisely known energies from Ref. [6], the positions of the peaks were constrained. These constraints were important to avoid overfitting the spectrum.

A further assumption made, based again on the spectra from Ref. [6], was that those states seen only weakly in that study would also be weakly populated in this experiment and on this basis they could be omitted from the fitting procedure, for instance, the 7154(5)-keV state. An example of a fit around the astrophysical region of interest is shown in Fig. 3, with those states included in the fit given in Table I.

From these measurements, the resulting differential yield could be compared to adiabatic distorted-wave approximation (ADWA) predictions of differential cross sections [14]. ADWA was chosen over distorted-wave Born approximation (DWBA) predictions as the beam energy was high enough that deuteron breakup effects need to be accounted for [15]. The code FRESCO was used for both ADWA and DWBA calculations [16]. Although the energy was only just above the recommended limit for DWBA, it was found that ADWA analysis produced a marginally better fit for states with previously determined spin parities, such as the prominent 6609-keV state below the neutron threshold. A comparison of DWBA and ADWA will be presented in the Results sections.

To deduce which ℓ transfer was associated with each energy level in the ^{20}Ne$(d, p)^{21}$Ne reaction, predictions for several possible spin parities were trialed against the data for each energy level in turn. The spin-parity assignments were made by comparing ADWA predictions to the data and selecting the ℓ transfer which gave the best fit. χ^2 minimization was only used as a guide in determining the angular momentum transferred due to correlations between data points.

As the measurements at different angles were simultaneous, the shape of the differential cross section is replicated without converting observed yield to the differential cross section. The efficiencies of the Si detectors were assumed to be identical. The solid angle coverage of each detector did vary, however, and was calculated using geometry and kinematics. The solid angle for each detector was then normalized to that of the detectors at the second angular position (detectors 1, 7, 13, and 19).

It was decided to use only a single detector from the four at each angle, choosing the detector with the best resolution of the four. This decision favored improved detector resolution by sacrificing counts. It also introduced an additional uncertainty in the measured counts originating in a misalignment of the beam along the beam axis which was quantified

TABLE I. Results from the HELIOS ^{20}Ne$(d, p)^{21}$Ne experiment. The breaks in the table indicate the neutron threshold at 6761.16(4) keV and the alpha threshold at 7347.93(4) keV [18].

E_x (keV)	ℓ_n	$2J^\pi$	$2J^\pi$ lit.[a]	$(2J+1)S_f$[b]	$(2J+1)S_f$ lit.[c]	Γ_n (eV)	$\Gamma_n$lit. (eV)[d]
2794	0	1^+	1^+	0.981 ± 0.186			
	3	$(5, 7)^-$		$3.782 \pm 0.695, 4.187 \pm 0.766$			
4526	2	$(3, 5)^+$	5^+	$1.024 \pm 0.240, 1.146 \pm 0.260$	1.56		
4725	2	$(3, 5)^+$	3^-	$3.476 \pm 0.703, 3.890 \pm 0.779$	3.19		
5334	2	$(3, 5)^+$	5^+ or 7^-	$2.591 \pm 0.567, 2.909 \pm 0.621$	0.84		
5549	2	$(3, 5)^+$	3^+	$1.143 \pm 0.183, 1.280 \pm 0.716$	0.74		
5822	3	$(5, 7)^-$	3^+	$0.703 \pm 0.149, 0.792 \pm 0.167$	0.34		
	2	$(3, 5)^+$		$0.548 \pm 0.102, 0.616 \pm 0.113$			
6609	2	$(3, 5)^+$	$(3, 5)^+$	$0.884 \pm 0.147, 1.000 \pm 0.160$	1.00		
7108	2	$(3, 5)^+$	$(3, 5)^+$	$0.099 \pm 0.029, 0.110 \pm 0.033$		220(60), 150(40)	160(20), 630(90)
	3	$(5, 7)^-$	or $(5, 7)^-$				2.9(2), 2.5(2)
7176	2	$(3, 5)^+$	$(3, 5)^+$	$0.265 \pm 0.042, 0.297 \pm 0.046$		950(100), 630(60)	300(20), 220(20)
7337	3	$(5, 7)^-$	$(3, 5)^+$	$0.205 \pm 0.047, 0.231 \pm 0.052$		30(5), 23(4)	960(50), 960(80)
7420		Undetermined	$(5, 7)^-$				4(1), 11(1)
7559	1	$(1, 3)^-$	$(3, 5)^+$	$0.036 \pm 0.006, 0.042 \pm 0.008$		15800(1900), 8000(1200)	570(30), 420(20)
7619	1	$(1, 3)^-$	3^-	$0.043 \pm 0.007, 0.051 \pm 0.009$		23200(2800), 11800(1600)[e]	8000(1000)
7749		Undetermined	5^+			$\leqslant 9300$	200(140)
7820	1	$(1, 3)^-$	$(3, 5)^+$	$0.028 \pm 0.008, 0.034 \pm 0.009$		22900(6000), 12200(2900)	560(90), 400(60)
7981	6	$(11, 13)^+$	3^-	$1.473 \pm 0.204, 1.547 \pm 0.221$			14000(5000)
	5	$(9, 11)^-$		$0.263 \pm 0.048, 0.295 \pm 0.053$			

[a]Literature values are taken from Ref. [13] below 6.0 MeV and from Refs. [6,19] above 6.0 MeV.
[b]Results are normalized to 6609 keV with $2J^\pi = 5^+$.
[c]Ref. [12].
[d]Refs. [6,19].
[e]Results for $2J^\pi = 3^-$ are used to compare to literature results [6] and estimate other partial widths.

as 10%, by calculating the percentage of the total counts measured by each of the four sides of the array. The uncertainty arising from the beam offset is not included in the error bars when plotting differential cross sections.

Without the measurements necessary to calculate absolute cross sections, only the relative spectroscopic factors of each state could be determined. Each spectroscopic factor is reported as relative to 6609 keV. This allowed comparison with previous studies [12]. The neutron widths could also not be directly determined without the absolute cross sections but, by scaling the relative spectroscopic factors from this study to those found by Ref. [6], an attempt was made to assign upper limits.

Estimating partial widths

The data from HELIOS were used to calculate a scaling factor (S_f) that could compare theoretical cross sections to proton counts. It is important to note here that the scaling factor S_f has no physical meaning. The number of counts is measured on an arbitrary scale and to convert to an experimental cross section would require reliable measurements of beam intensity which, without appropriate scattering data, can only be estimated to around a factor of 2 uncertainty.

However, given the importance of the neutron partial widths in calculating the rates of reaction for ^{17}O$(\alpha, n)^{20}$Ne for nuclear astrophysics, it was highly desirable to provide estimates for the widths. This was achieved using the TUNL data as a point of reference and scaling the HELIOS S_f to C^2S. From there Γ_n was calculated. The method first defined $C^2S_{\text{TUNL}} = C^2S_{\text{HELIOS}} = \kappa \times S_f$ with κ containing the missing experimental information. Then κ was evaluated using the 7619-keV state, for which the HELIOS and TUNL spin-parity results both found $J^\pi = \frac{3}{2}^-$ as the best fit for their respective data. Now with a value for κ, the spectroscopic factor for the HELIOS data was calculated as $C^2S_{\text{HELIOS}} = \kappa \times S_f$. The differential cross section ($\frac{d\sigma}{d\Omega}$) was then calculated by multiplying the measured counts per steradian as measured by HELIOS with C^2S_{HELIOS}. With an estimate for differential cross sections now in the correct units, partial widths could be calculated using Eq. (2.162) from Ref. [17]. The difference in center-of-mass energy between the two experiments should be accounted for in the FRESCO calculations.

IV. RESULTS

The difference between ADWA and DWBA predictions for the 6609-keV state is shown in Fig. 4, comparing predictions for $\ell = 2$ and 3 to data. According to previous studies [6], this state has a spin parity of $2J^\pi = (3, 5)^+$ which implies an $\ell = 2$ transfer. The ADWA predictions exclude an $\ell = 3$ transfer, thus showing ADWA could more reliably reproduce literature values than DWBA in the present work.

The results from the fitting of the ADWA to the data are summarized in Table I which lists the $\Delta\ell$ and J^π assignments as well as the spectroscopic factors of each state relative to the 6609-keV state. Using the 6609-keV state to normalize the data allows for comparison with literature such

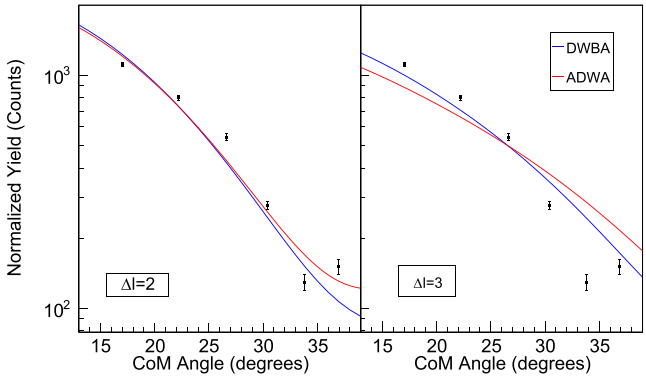

FIG. 4. A comparison of two different ℓ transfers predicted for the 6609-keV energy level (left is $\ell = 2$, right is $\ell = 3$) to illustrate the improved fit of ADWA model predictions (red) over DWBA model predictions (blue). A state with a known spin parity of $J^\pi = (\frac{3}{2}, \frac{5}{2})^+$ implies an $\ell = 2$ transfer in a (d, p) reaction.

as Refs. [12,20] which also reported the spectroscopic factor in this manner. The most up-to-date values for alpha partial widths are not included in the table, but can be found in Ref. [8].

After the 7980-keV state, the energy level density is sufficiently high that, with the resolution of HELIOS, analysis of individual levels was not possible, therefore this is the last energy level that was analyzed in the present work.

A. States below the neutron threshold

The results for the 2794, 4526, 4725, 5334, 5549, 5822 and 6609 keV states are shown in Figs. 5–11, respectively. The 2794-keV energy level was the lowest energy state investigated in this study. The 2794-keV state sits at the low-energy limit of the kinematic acceptance of HELIOS at this magnetic field strength and beam energy, with the higher angle data missing. The detectors that did observe the 2794-keV state were used to plot Fig. 5. Two possible ℓ transfers fit these

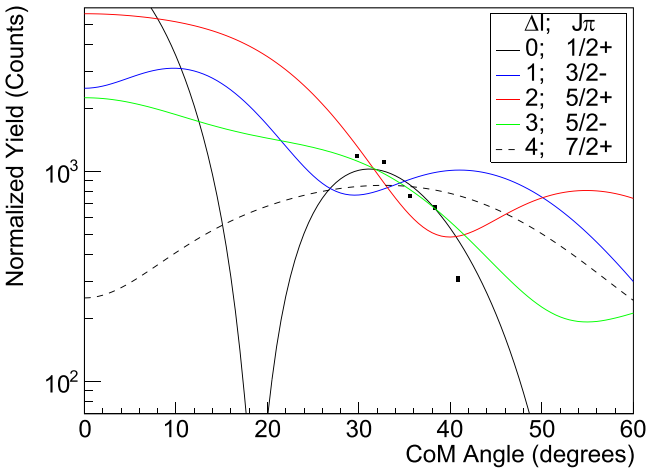

FIG. 5. Measured differential cross section for the 2794-keV energy level compared to different ℓ-transfer predictions. The best fitting prediction is $\ell = 0$.

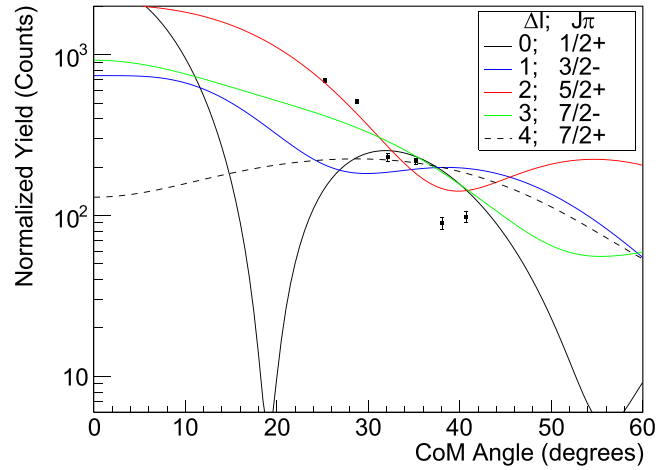

FIG. 6. Measured differential cross section for the 4526-keV energy level compared to different ℓ-transfer predictions. The best fitting prediction is $\ell = 2$.

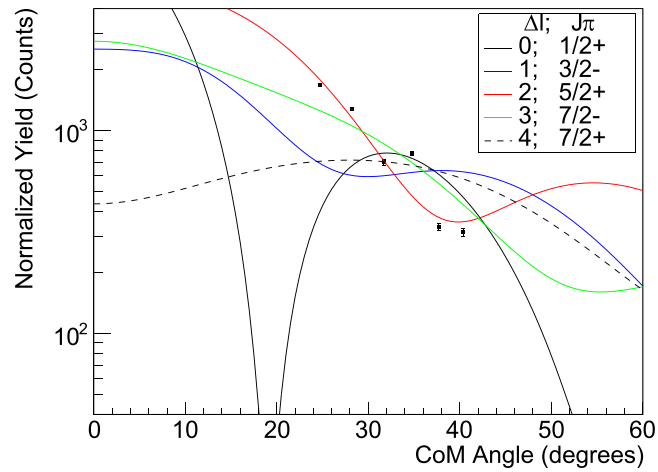

FIG. 7. Measured differential cross section for the 4725-keV energy level compared to different ℓ-transfer predictions. The best fitting prediction is $\ell = 2$.

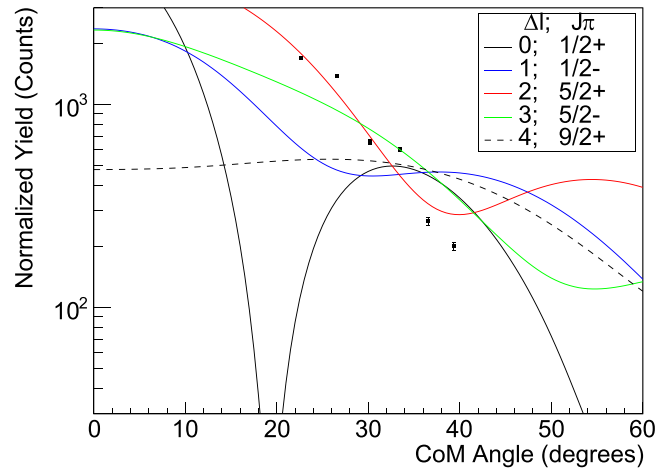

FIG. 8. Measured differential cross section for the 5334-keV energy level compared to different ℓ predictions. The best fitting prediction is $\ell = 2$.

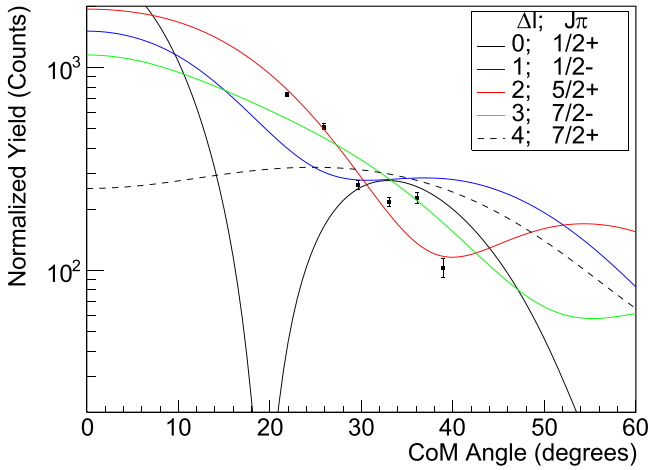

FIG. 9. Measured differential cross section for the 5549-keV energy level compared to different ℓ-transfer predictions. The best fitting prediction is $\ell = 2$.

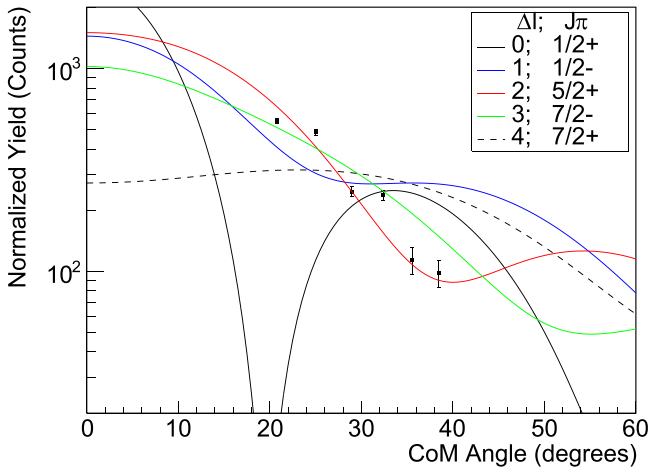

FIG. 10. Measured differential cross section for the 5822-keV energy level compared to different ℓ-transfer predictions. The best fitting predictions are $\ell = 2$ and 3.

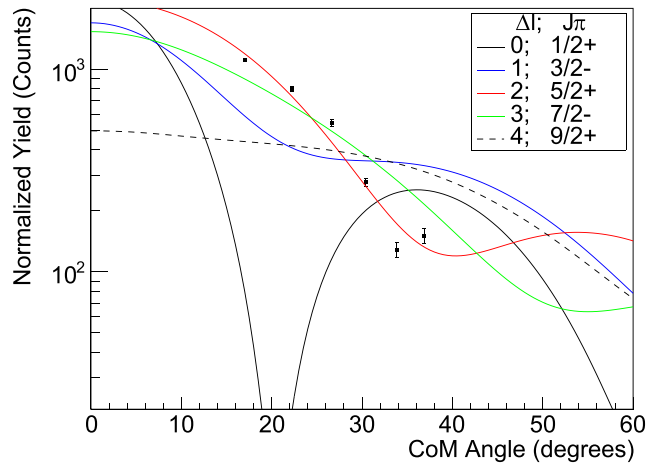

FIG. 11. Measured differential cross section for the 6609-keV energy level compared to different ℓ-transfer predictions. The best fitting prediction is $\ell = 2$.

data: $\ell = 0$ and 3, which would imply either $2J^\pi = 1^+$ or $(5, 7)^-$, respectively. Previous studies also report a spin parity of $2J^\pi = 1^+$ for this state [20,21]. These data, however, cannot rule out $\ell = 3$, therefore those results are shown in Table I.

The 4526-, 5549-, and 6609-keV states were all best fit with an $\ell = 2$ transfer, implying spin parity of either $2J^\pi = 3^+$ or 5^+. These assignments concur with previous results from experiments studying various reactions: Refs. [12,20,22] for 4526 keV, Refs. [20,21] for 5549 keV, and Ref. [6] for 6609 keV. The 6609-keV state, being well separated from other strongly populated states, is often used to normalize the spectroscopic factors of other states. For the purpose of comparing to literature, the scaling factors from this study have been normalized to that of the 6609-keV state assuming $J^\pi = \frac{5}{2}^+$.

These data for the 4725-keV state best fit a transfer of $\ell = 2$. Such a transfer would imply a spin parity of $2J^\pi = (3, 5)^+$. This is in disagreement with a previous ^{20}Ne$(d, p)\,^{21}$Ne study, which reported $2J^\pi = 3^-$ [12] for this state.

The data for the 5334-keV state best fit an $\ell = 2$ transfer, resulting in a spin-parity assignment of $2J^\pi = (3, 5)^+$, as shown in Fig. 8. This is in disagreement with the value reported in an ^{17}O$(^7$Li$, np\gamma)\,^{21}$Ne experiment [23]. However, other studies using multiple reactions, such as ^{20}Ne$(d, p)\,^{21}$Ne [20] and ^{18}O$(\alpha, n\gamma)\,^{21}$Ne [24], have previously found $2J^\pi = (3, 5)^+$ as well and these results are in agreement with those findings.

The analysis of the data from the 5822-keV state, shown in Fig. 10, could not distinguish between a transfer of $\ell = 2$ and 3. The shapes of both transfers in the angular region studied are quite similar for many of the states investigated, and in this case neither could be reliably excluded. The resulting assignment for spin parity is either $2J^\pi = (3, 5)^+$ or $(5, 7)^-$. Previous studies assign $2J^\pi = 3^+$ as the spin parity [20,25], thus we assume $2J^\pi = 3^+$.

B. 7108 and 7176 keV

These two states appear as one wide peak on the spectrum since they are close in excitation energy and therefore are difficult to resolve. It was found for 7108 keV that either a transfer of $\ell = 2$ or $\ell = 3$ best fit the data, as shown on Fig. 12. This resulted in a spin-parity assignment of $2J^\pi = (3, 5)^+$ or $(5, 7)^-$, which is in agreement with the previous ^{20}Ne$(d, p)\,^{21}$Ne study which also could not discriminate between an $\ell = 2$ or 3 transfer. The 7176 keV state also yielded a best fit of $\ell = 2$, as shown on Fig. 13. However, that assignment disagrees with the TUNL study that first reported this state as having a spin parity of $2J^\pi = (1, 3)^-$. A possible reason for this discrepancy is that, being unresolved from one another, counts from one peak are being erroneously included in the fits for the other, thus impacting the ADWA analysis. Another explanation may lie in the assumptions made during analysis. When fitting above the neutron threshold, several energy levels were treated as negligible since they were not strongly populated during the TUNL experiment [19]. Since that experiment took place at a lower center-of-mass energy that was used in this experiment, it is possible that one or more of those energy levels were more strongly populated

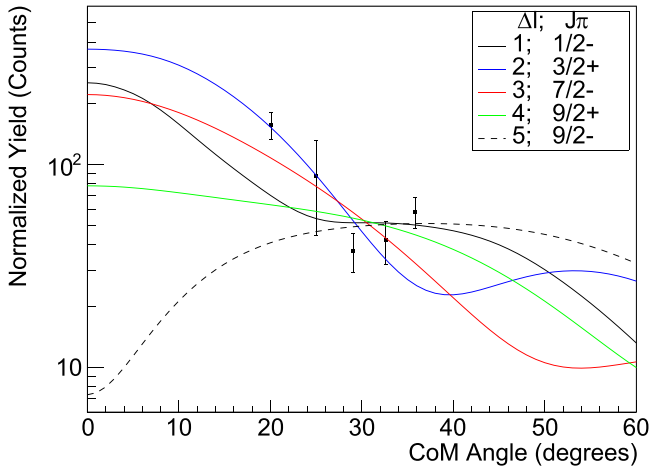

FIG. 12. Measured differential cross section for the 7108-keV energy level compared to the five best fitting ℓ-transfer predictions. The best fitting prediction is $\ell = 2$ or 3.

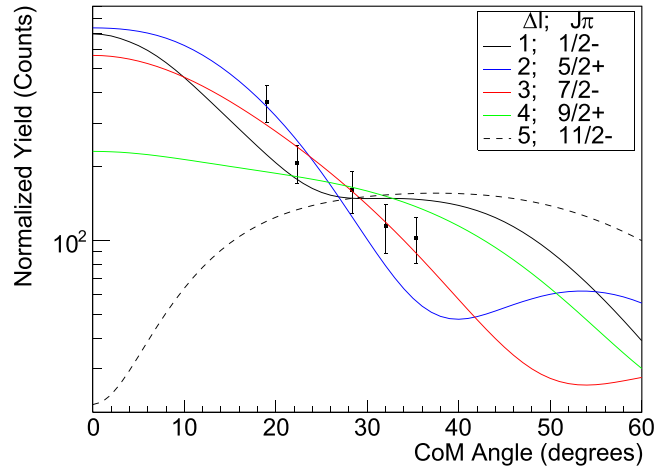

FIG. 14. Measured differential cross section for the 7337-keV energy level compared to the five best fitting ℓ-transfer predictions. The best fitting prediction is $\ell = 3$.

in this experiment than assumed. Such a state (for instance the 7156-keV state) could potentially contribute to the counts under the unresolved 7108- and 7176-eV peak.

C. 7337 and 7420 keV

These states are also unresolved in the spectra measured with HELIOS. The best fitting transfer for 7337 keV is shown on Fig. 14 as $\ell = 3$, disagreeing with the TUNL study that assigned $\ell = 1$. The data for the 7420-keV state fit three possible transfers: $\ell = 1,\ 2,$ or 3 preventing a reliable spin-parity assignment for this state. The overlap between the 7420- and the 7337-keV states could be the reason for the shape of the angular distribution, shown in Fig. 15. The (d, p) study of Ref. [6] and the (^{7}Li, t) study of Ref. [8] both found high spins for this state, with Ref. [6] favoring a $2J^\pi = 5^-$ or 7^- assignment, while Ref. [8] favored an assignment of $2J^\pi = 11^-$. The latter assignment agrees with previous (^{7}Li, np) studies by Refs. [22,23].

D. 7559 keV

These data find the best fitting transfer for 7559 keV to be $\ell = 1$. The TUNL experiment found that their data could either fit $\ell = 1$ or 2 however they reported $\ell = 2$ since the larger neutron width associated with an $\ell = 1$ should have been observed in previous neutron resonance studies and was not [26]. Reference [8] found that $2J^\pi = 5^+$ for this state provided a good fit to their data, which supports the TUNL assignment. As seen in Fig. 16, $\ell = 2$ does not give a good fit to these data and therefore $\ell = 1$ must be reported here as the best fitting transfer, despite the disagreements with the other studies. The scale of the error bars in this data comes from a combination of low statistics, low resolution, and the

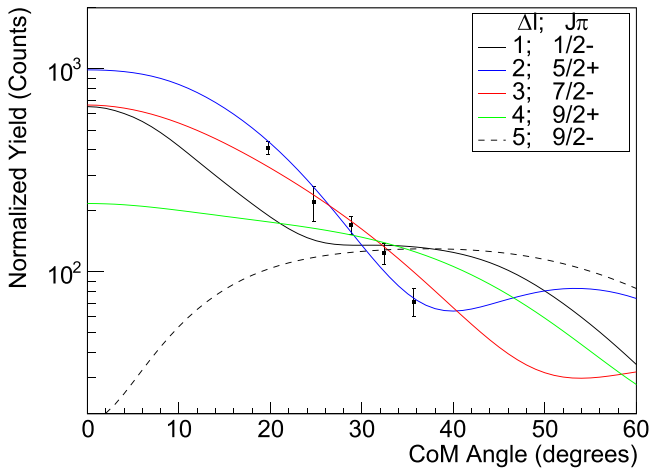

FIG. 13. Measured differential cross section for the 7176-keV energy level compared to the five best fitting ℓ-transfer predictions. The best fitting prediction is $\ell = 2$.

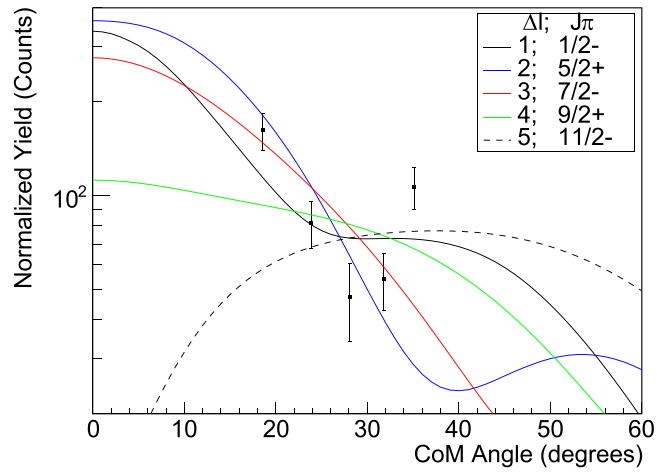

FIG. 15. Measured differential cross section for the 7420-keV energy level compared to the five best fitting ℓ-transfer predictions. None of the predictions fit these data well.

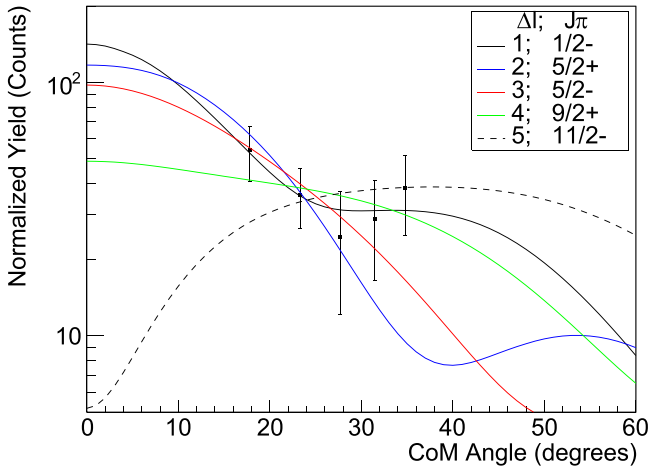

FIG. 16. Measured differential cross section for the 7559-keV energy level compared to the five best fitting ℓ-transfer predictions. The best fitting prediction is $\ell = 1$.

proximity of this state to other more prominent states nearby (the 7420- and 7619-keV states).

E. 7619 keV

This study found that a transfer of $\ell = 1$ best fit the data for the 7619 keV state, as shown on Fig. 17, implying a spin parity of $2J^\pi = (1, 3)^-$. The 7619-keV state has now been consistently assigned $2J^\pi = 3^-$ over four studies, each using different experimental methods. Since this state was above the neutron threshold and in good agreement with the TUNL study, it was chosen for use in estimating partial widths, as discussed in the Data Analysis section. While the $2J^\pi$ assignment is not contentious, there is a marginal disagreement in the values for neutron partial width between the (d, p) study of Ref. [6] and the neutron resonance study of Ref. [26]. This is worth highlighting for the later discussion on the 7820-keV state.

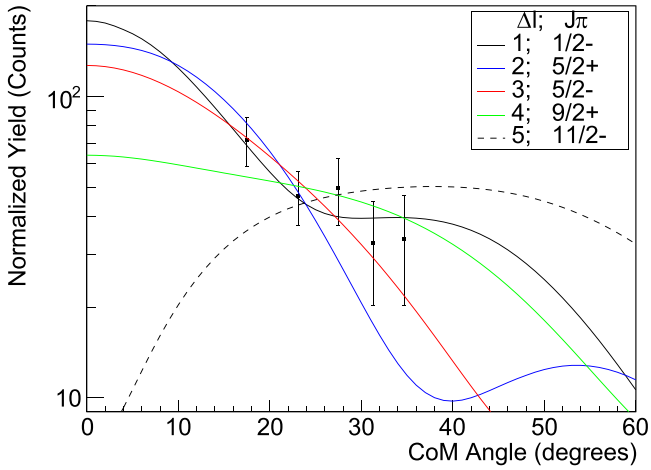

FIG. 17. Measured differential cross section for the 7619-keV energy level compared to the five best fitting ℓ-transfer predictions. The best fitting prediction is $\ell = 1$.

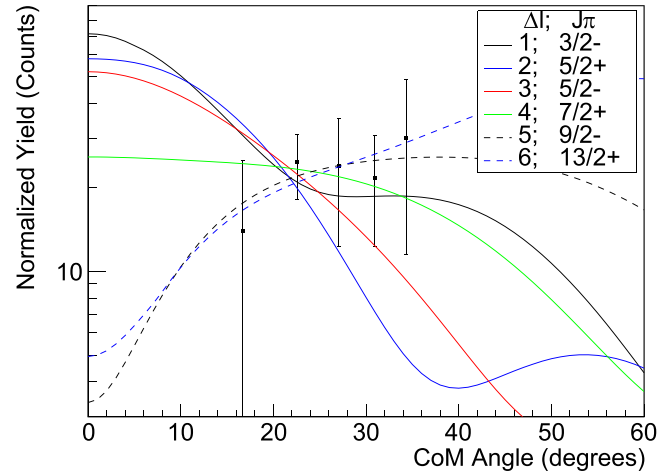

FIG. 18. Measured differential cross section for the 7749-keV energy level compared to all ℓ-transfer predictions trialed (except $\ell = 0$). The large uncertainties on the measurements mean that many predictions fit these data.

F. 7749 keV

Unfortunately, this study was unable to determine the ℓ transfer for this state, the data for which are consistent with being flat, as shown in Fig. 18. The flat shape of the differential cross section could suggest that other reaction mechanisms are contributing to the cross section for this state. In this case, ADWA analysis would not be able to fully represent the ongoing physics in the reaction. The only ℓ transfer that could be excluded from these data was $\ell = 2$.

Since this state is above the neutron threshold, it is unlikely to be $\ell = 0$ based on the TUNL data, which found it to be a narrow peak. Without either a Coulomb barrier or an angular momentum barrier, states at these energies with $2J^\pi = 1^+$ are expected to be broad, such as is the case for the 7211-keV state [27]. The minimum possible transfer is therefore assumed to be $\ell = 1$. Under this assumption an estimate for the partial width with $2J^\pi = 1^-$ was $\Gamma_n = 12\,700(6100)$ eV. Since Ref. [6] observed this state at one angle as being narrow, this value for the experimental width is too large. Trialing instead $2J^\pi = 3^-$, the partial width was calculated to be 6400(2900) eV. This would be consistent with the experimental width from Ref. [6] and therefore the upper limit for the neutron width of the 7749-keV state is $\Gamma_n \leqslant 9300$ eV.

The limit for the resonance strength, assuming $2J^\pi = 3^-$ and the alpha widths in Ref. [28], was calculated to be $\omega\gamma_n < 14.7 \times 10^{-3}$ μeV, where $\omega = \frac{(2J_r+1)}{(2J_1+1)(2J_2+1)}$ and the assumption that $\Gamma_\alpha << \Gamma_{n,\gamma}$ is made. Reference [28] estimated a resonance strength of 0.022 μeV, which is close to this result.

Multiple experiments have now failed to deduce the spin parity of this state, and it remains a source of uncertainty in models of the weak *s* process.

G. 7820 keV

This study finds the best fitting transfer for the 7820-keV state was $\ell = 1$. The data from the TUNL experiment [6] fit both $\ell = 1$ and 2, however they reported $\ell = 2$ despite

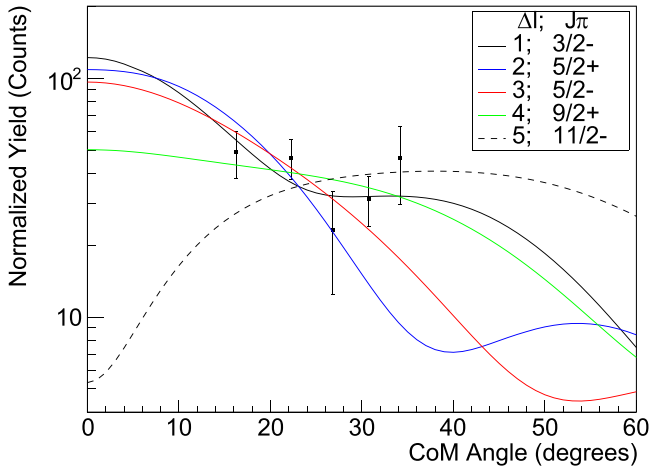

FIG. 19. Measured differential cross section for the 7820-keV energy level compared to the five best fitting ℓ-transfer predictions. The best fitting prediction is $\ell = 1$.

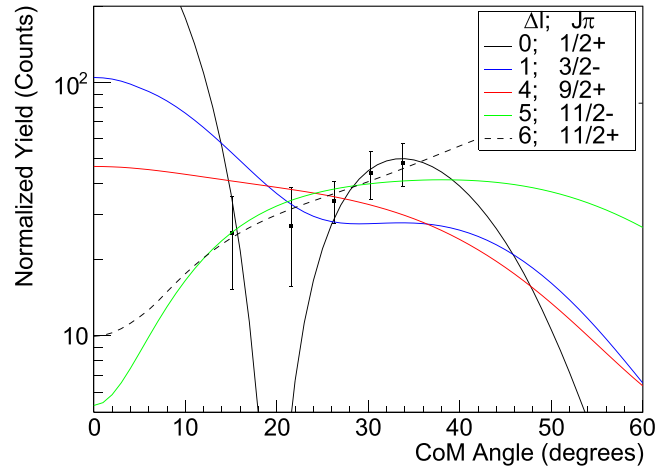

FIG. 20. Measured differential cross section for the 7980-keV energy level compared to the five best fitting ℓ-transfer predictions. The best fitting predictions are $\ell = 5$ and 6.

1 giving a slightly better fit. The justification for that decision was that an $\ell = 1$ transfer would have produced a large neutron width, something that had not been reported in an earlier neutron resonance experiment [26]. It is worth noting, however, that for the 7619-keV level the neutron partial widths reported by Refs. [6,26] are not in agreement. In any case, an $\ell = 2$ transfer does not fit these data well; as can be seen in Fig. 19 the best fitting ADWA prediction is $\ell = 1$. A recent ^{17}O(^{7}Li, t)^{21}Ne study found a best fitting spin parity of ($2J^{\pi} = 7^{-}$), which in a (d, p) reaction would produce an $\ell = 3$ transfer. Such an assignment would be consistent with the neutron resonance experiment, however this highlights a disagreement between those experiments and the two (d, p) experiments conducted at TUNL and ANL. The uncertainty surrounding this state has significant repercussions when estimating reaction rates for the weak s process.

Assuming $\ell = 1$ these data were used to calculate neutron partial widths for the two possible spin parities of $\Gamma_n = 22\,900 \pm 6000$ and $12\,200 \pm 2900$ eV for $2J^{\pi} = 1^{-}$ and 3^{-}, respectively. Since Ref. [6] observed this state to be narrower than their experimental resolution (FWHM = 10 keV), the higher partial width can be excluded resulting in a spin-parity assignment of $2J^{\pi} = 3^{-}$ with an associated width of $\Gamma_n = 12\,200 \pm 2900$ eV. It is possible that in the neutron resonance study of Ref. [26], the large granularity of measurements at these excitation energies resulted in that experiment missing this state.

The resonance strength using this updated spin parity and the alpha width from Ref. [28] is $\omega\gamma_n = 0.36\,\mu$eV and is a third lower than reported in Ref. [28]. Reference [8] reported a spin parity of $2J^{\pi} = 7^{-}$ and $\Gamma_{\alpha} = 15.7\,\mu$eV which would mean $\omega\gamma_n = 20.9\,\mu$eV, significantly higher than these data suggest. In either case, results from these data suggest that the ^{17}O(α, n)^{20}Ne reaction is less favorable; therefore, the s process is less efficient in rotating massive stars than would be the case in the previous studies.

H. 7980 keV

The 7982.1- and 7980-keV states form a doublet. However, because 7982.1 keV has a reported $2J^{\pi} = (7, 11)^{+}$ [25], it is expected that counts in this study will be dominated by the 7980-keV state. Such a spin parity would mean an ℓ transfer of 4 or 6 for the 7982.1-keV state and those transfers are not expected to be significantly populated in a ^{20}Ne(d, p)^{21}Ne experiment. The analysis of these data, shown in Fig. 20, indicate a best fitting ℓ transfer of 5 or 6. Reference [6] reported a transfer of $\ell = 1$, for which the study by Ref. [8] is in agreement with their assignment of $2J^{\pi} = 3^{-}$ to this state. Therefore this study is in disagreement. This could arise from the poor separation of this state from the nearby 8068-keV state in the HELIOS data, or perhaps 7982.1 keV is contributing more to the peak than was assumed.

I. Other energy levels

Those energy levels within the astrophysical energy range of interest for the weak s process, but not reported in these data, shall now briefly be discussed here. Above 7981 keV, there is little disagreement between the available literature for the known states, as shown in Table II. For the 7960- and 7655.7-keV states as well, those experiments that have observed these states concur that their spin parities are $2J^{\pi} = 11^{-}$ and 7^{+}, respectively. The results for 7420 keV as well are uncontentious with both (d, p) [6] and (d, t) [29] studies reporting $2J^{\pi} = (1, 3)^{-}$ and more recently an (^{7}Li, t) experiment [8] finding $2J^{\pi} = 3^{-}$. The (d, p) study of Ref. [6] identified a weakly populated state at 7602 keV, but could not distinguish between an ℓ transfer of 3 or 4 for the state. Again, combining the results from the recent (^{7}Li, t) study supports an assignment of $2J^{\pi} = 7^{-}$.

J. Conclusion

A ^{20}Ne(d, p)^{21}Ne experiment motivated by reducing the uncertainties in the weak s process was conducted at ANL using the HELIOS spectrometer. Spin parities have been

TABLE II. A summary of the results from the available literature studying the astrophysically relevant energy levels of ^{21}Ne. J^π values in brackets are tentative assignments.

E_x (keV)	E_{res} (keV)	Source	Experiment	$2J^\pi$	Γ_n (eV)
7420.4(15)	72.5	[23]	^{16}O(^{7}Li, np)^{21}Ne	11^-	
		[22]	^{16}O(^{7}Li, np)^{21}Ne	$(9, 11)^-$	
		[6]	^{20}Ne(d, p) ^{21}Ne	$(5, 7)^-$	14(1), 11(1)
		[8]	^{17}O(^{7}Li, t) ^{21}Ne	11^-	
7470(2)	122	[29]	^{22}Ne(d, t) ^{21}Ne	$(1, 3)^-$	
		[6]	^{20}Ne(d, p) ^{21}Ne	$(1, 3)^-$	
		[8]	^{17}O(^{7}Li, t) ^{21}Ne	3^-	
7559.1(15)	211.2	This work	d(^{20}Ne , ^{21}Ne)p	$(1, 3)^-$	
		[6]	^{20}Ne(d, p) ^{21}Ne	(5^+)	570(30), 420(20)
		[8]	^{17}O(^{7}Li, t) ^{21}Ne	(5^+)	
7602.0(15)	254.1	[6]	^{20}Ne(d, p) ^{21}Ne	$(5, 7)^-$ or $(7, 9)^+$	8(2), 6(2) or 0.4(1), 0.3(1)
		[8]	^{17}O(^{7}Li, t) ^{21}Ne	7^-	
7619.9(10)	272.0	This work	d(^{20}Ne , ^{21}Ne)p	3^-	
		[6]	^{20}Ne(d, p) ^{21}Ne	3^-	8000(1000)
		[8]	^{17}O(^{7}Li, t) ^{21}Ne	3^-	
		[26]	Neutron res.	3^-	14000(4000)
7655.7(22)5	307.8	[25]	^{18}O(α, $n\gamma$) ^{21}Ne	7^+	
		[8]	^{17}O(^{7}Li, t) ^{21}Ne	7^+	
		[6]	^{20}Ne(d, p) ^{21}Ne	7^+	
7748.8(17)	400.9	This work	d(^{20}Ne , ^{21}Ne)p	Undetermined	<9300
		[6]	^{20}Ne(d, p) ^{21}Ne	Undetermined	
		[8]	^{17}O(^{7}Li, t) ^{21}Ne	Undetermined	
7820.1(15)	472.2	This work	d(^{20}Ne , ^{21}Ne)p	$(1, 3)^-$	12200(2900)
		[6]	^{20}Ne(d, p) ^{21}Ne	$(3, 5)^+$	560(90), 400(60)
		[8]	^{17}O(^{7}Li, t) ^{21}Ne	(7^-)	
7960(2)	612	[22]	^{16}O(^{7}Li, np)^{21}Ne	$11^{(-)}$	
		[6]	^{20}Ne(d, p) ^{21}Ne	11^-	
		[8]	^{17}O(^{7}Li, t) ^{21}Ne	11^-	
7981(2)	633	[26]	Neutron res.	3^-	6000(2000)
		[6]	^{20}Ne(d, p) ^{21}Ne	3^-	14000(5000)
		[8]	^{17}O(^{7}Li, t) ^{21}Ne	3^-	
7982.1(7)	634.2	[25]	^{18}O(α,$n\gamma$) ^{21}Ne	$(7, 11)^+$	
		[23]	^{16}O(^{7}Li, np) ^{21}Ne	11^+	
		[8]	^{17}O(^{7}Li, t) ^{21}Ne	(7^+)	
8008(2)	660	[26]	Neutron res.		32000(6000)
		[6]	^{20}Ne(d, p) ^{21}Ne	1^-	
		[8]	^{17}O(^{7}Li, t) ^{21}Ne	1^-	
8069(1)	721	[28]	^{17}O(α, n) ^{21}Ne	3^+	
		[26]	Neutron res.		8000(3000)
		[6]	^{20}Ne(d, p) ^{21}Ne	3^+	1600(200)
		[8]	^{17}O(^{7}Li, t) ^{21}Ne	3^+	
8146(1)	798	[28]	^{17}O(α, n) ^{21}Ne	3^+	
		[6]	^{20}Ne(d, p) ^{21}Ne	$(3, 5)^+$	550(150), 400(100)
		[8]	^{17}O(^{7}Li, t) ^{21}Ne	3^+	
8159(2)	811	[25]	^{18}O(α,$n\gamma$) ^{21}Ne	$9^?$	
		[6]	^{20}Ne(d, p) ^{21}Ne	9^+	
		[8]	^{17}O(^{7}Li, t) ^{21}Ne	(9^+)	
		[30]	^{17}O(α,γ) ^{21}Ne	5–11	
		[22]	^{16}O(^{7}Li, np) ^{21}Ne	$9^?$	
8160(2)	812	[28]	^{17}O(α, n) ^{21}Ne	5^+	
		[6]	^{20}Ne(d, p) ^{21}Ne	5^+	23000(2300)
8189	841	[28]	^{17}O(α, n) ^{21}Ne	3^-	

deduced for prominent states below the neutron threshold and for states important to astrophysics. Estimates for the neutron partial widths of certain important states have been made by way of a comparison to another, earlier (d, p) experiment. While the current literature favors some recycling of neutrons from ^{16}O poisoning [6,8], there remains uncertainty in the rate of weak *s*-process nucleosynthesis since spectroscopic parameters of several important states, especially 7820 and 7749 keV, remain missing or disputed.

DWBA (or, in this case, ADWA) predictions are generally able to reproduce measured data from direct reactions populating states in ^{21}Ne, and are usually in agreement across multiple reaction mechanisms, where high statistics are available.

Further experiments aimed at determining the spin parity and neutron partial widths for the 7749-keV state would assist in further reducing the uncertainty in the ratio of the $^{17}\mathrm{O}(\alpha, n)\,^{20}\mathrm{Ne}$ to $^{17}\mathrm{O}(\alpha,\gamma)\,^{21}\mathrm{Ne}$ reaction rates. Additionally, there is disagreement between studies that utilized different reaction mechanisms on the spin parity of the important 7820-keV state. Future studies aimed at resolving this disagreement also would be beneficial; in particular an updated neutron resonance experiment to confirm or refute current literature [26] may be able to better constrain possible spin parities. As the literature stands, the uncertainty surrounding these two energy levels introduces significant uncertainty in any estimates for *s*-process nucleosynthesis in rotating massive stars [6,8].

ACKNOWLEDGMENTS

This material is based upon work supported by the U.S. Department of Energy (DOE), Office of Science, Office of Nuclear Physics, under Contract No. DE-AC02-06CH11357. This research used resources of ANL's ATLAS facility, which is a DOE Office of Science User Facility. A.M.L. and J.F.-S. acknowledge the support of the UK Science and Technology Facilities Council. This paper is based upon work from the "ChETEC" COST Action (CA16117), supported by COST (European Cooperation in Science and Technology). C.A. acknowledges the generous support of the Natural Sciences and Engineering Research Council of Canada. TRIUMF receives federal funding via a contribution agreement through the National Research Council of Canada.

DATA AVAILABILITY

The data supporting this study's findings are available within the article.

[1] F. Käppeler, R. Gallino, S. Bisterzo, and W. Aoki, Rev. Mod. Phys. **83**, 157 (2011).
[2] M. Pignatari, R. Gallino, G. Meynet, R. Hirschi, F. Herwig, and M. Wiescher, Astrophys. J. **687**, L95 (2008).
[3] F. Rizzuti, G. Cescutti, F. Matteucci, A. Chieffi, R. Hirschi, M. Limongi, and A. Saro, Mon. Not. R. Astron. Soc. **502**, 2495 (2021).
[4] C. Travaglio, R. Gallino, E. Arnone, J. Cowan, F. Jordan, and C. Sneden, Astrophys. J. **601**, 864 (2004).
[5] A. Choplin, R. Hirschi, G. Meynet, S. Ekström, C. Chiappini, and A. Laird, A&A **618**, A133 (2018).
[6] J. Frost-Schenk, P. Adsley, A. M. Laird, R. Longland, C. Angus, C. Barton, A. Choplin, C. A. Diget, R. Hirschi, C. Marshall, F. Portillo-Chaves, and K. Setoodehnia, Mon. Not. R. Astron. Soc. **514**, 2650 (2022).
[7] M. Molero, L. Magrini, F. Matteucci, D. Romano, M. Palla, G. Cescutti, C. V. Vázquez, and E. Spitoni, Mon. Not. R. Astron. Soc. **523**, 2974 (2023).
[8] F. Hammache, P. Adsley, L. Lamia, D. S. Harrouz, N. de Séréville, B. Bastin, A. Choplin, T. Faestermann, C. Fougères, R. Hertenberger, R. Hirschi, M. La Cognata, A. Meyer, S. Palmerini, R. G. Pizzone, F. de Oliveira Santos, S. Romano, A. Tumino, and H.-F. Wirth, Phys. Rev. Lett. **132**, 182701 (2024).
[9] C. Marshall, K. Setoodehnia, K. Kowal, F. Portillo, A. E. Champagne, S. Hale, A. Dummer, and R. Longland, IEEE Trans. Instrum. Meas. **68**, 533 (2019).
[10] J. Lighthall, B. Back, S. Baker, S. Freeman, H. Lee, B. Kay, S. Marley, K. Rehm, J. Rohrer, J. Schiffer, D. Shetty, A. Vann, J. Winkelbauer, and A. Wuosmaa, Nucl. Instrum. Methods Phys. Res. Sect. A **622**, 97 (2010).
[11] A. Wuosmaa, J. Schiffer, B. Back, C. Lister, and K. Rehm, Nucl. Instrum. Methods Phys. Res. Sect. A **580**, 1290 (2007).
[12] A. Stanford and P. Quin, Nucl. Phys. A **342**, 283 (1980).
[13] N. N. D. Centre, ENSDF, NNDC online data service, ENSDF database (2015), http://www.nndc.bnl.gov/ensdf/.
[14] G. L. Wales and R. Johnson, Nucl. Phys. A **274**, 168 (1976).
[15] S. Giron, Etude de la réaction d'intrt astrophysique ^{60}Fe (n, γ) ^{61}Fe par réaction de transfert (d, p), Ph.D. thesis, Université Paris Sud Paris XI, 2011.
[16] I. Thompson, Comput. Phys. Rep. **7**, 167 (1988).
[17] C. Iliadis, Nucl. Phys. A **618**, 166 (1997).
[18] M. Wang, G. Audi, A. H. Wapstra, F. G. Kondev, M. MacCormick, X. Xu, and B. Pfeiffer, Chin. Phys. C **36**, 1603 (2012).
[19] C. Angus, J. Frost-Schenk, A. M. Laird, P. Adsley, R. Longland, C. J. Barton, C. A. Diget, C. Marshall, F. Portillo Chaves, and K. Setoodehnia, Phys. Rev. C **109**, 044323 (2024).
[20] A. J. Howard, J. Pronko, and C. Whitten, Nucl. Phys. A **152**, 317 (1970).
[21] H. T. Fortune, J. D. Garrett, and R. Middleton, Phys. Rev. C **19**, 1615 (1979).
[22] S. Thummerer, W. von Oertzen, T. Kokalova, H. G. Bohlen, B. Gebauer, A. Tumino, T. N. Massey, G. de Angelis, M. Axiotis, A. Gadea, T. Kröll, N. Marginean, D. R. Napoli, M. D. Poli, C. Ur, D. Bazzacco, S. M. Lenzi, C. R. Alvarez, S. Lunardi, R. Menegazzo *et al.*, J. Phys. G **29**, 509 (2003).
[23] C. Wheldon, T. Kokalova, S. Thummerer, H. G. Bohlen, B. Gebauer, A. Tumino, T. N. M. ad G. de Angelis, M. Axiotis, A. Gadea, T. Kröll, N. Marginean, D. R. Napoli, M. D. Poli, C. Ur, D. Bazzacco, S. M. Lenzi, C. R. Alvarez, R. Menegazzo, P. G. Bizzeti, and A. M. Bizzeti-Sona, Eur. Phys. J. A **26**, 321 (2005).
[24] C. Rolfs, H. P. Trautvetter, E. Kuhlmann, and F. Riess, Nucl. Phys. A **189**, 641 (1972).

[25] A. Hoffman, P. Betz, H. Röpke, and B. H. Wildenthal, Z. Phys. A **332**, 289 (1989).
[26] H. O. Cohn and J. L. Fowler, Phys. Rev. **114**, 194 (1959).
[27] M. Heil, R. Plag, E. Uberseder, R. Gallino, S. Bisterzo, A. Juseviciute, F. Käppeler, C. Lederer, A. Mengoni, and M. Pignatari, Phys. Rev. C **90**, 045804 (2014).
[28] A. Best, M. Beard, J. Görres, M. Couder, R. deBoer, S. Falahat, R. T. Güray, A. Kontos, K.-L. Kratz, P. J. LeBlanc, Q. Li, S. O'Brien, N. Özkan, M. Pignatari, K. Sonnabend, R. Talwar, W. Tan, E. Uberseder, and M. Wiescher, Phys. Rev. C **87**, 045805 (2013).
[29] G. Mairle, L. K. Pao, G. J. Wagner, K. T. Knöpfle, and H. Riedesel, Z. Phys. A **301**, 157 (1981).
[30] A. Best, J. Görres, M. Couder, R. deBoer, S. Falahat, A. Kontos, P. J. LeBlanc, Q. Li, S. O'Brien, K. Sonnabend, R. Talwar, E. Uberseder, and M. Wiescher, Phys. Rev. C **83**, 052802(R) (2011).